Diffuse X-ray scattering from partially transformed 3C-SiC single crystals

D. Dompoint, Alexandre Boulle, I.G. Galben-Sandulache, D. Chaussende

Diffuse X-ray scattering from partially transformed 3C-SiC single crystals

D. Dompoint [a], A. Boulle [a], I. G. Galben-Sandulache [b], D. Chaussende [b]

[a]Science des Procédés Céramiques et de Traitements de Surface (SPCTS) CNRS UMR 6638

Centre Européen de la Céramique, 12 rue atlantis, 87068 Limoges, France

[b] Laboratoire des Matériaux et du Génie Physique (LMGP) CNRS UMR 5628, Grenoble INP, Minatec,

3 parvis Louis Néel, BP 257, 38016 Grenoble Cedex 01, France

Abstract. The 3C-6H polytypic transition in 3C-SiC single crystals is studied by means of diffuse X-ray scattering (DXS) coupled with numerical simulations. It is shown that the presence of spatially correlated stacking faults (characteristic of this type of re-stacking transition) gives rise to extended diffuse scattering in the reciprocal space perpendicularly to the fault plane. The simulation of the diffuse intensity allows to determine both the volume fraction of transformed material and the transformation level within these regions. It is further shown that the evolution with time and temperature of the transition implies the multiplication and glide of partial dislocations, the kinetics of which are quantified by means of DXS.

Keywords: Silicon carbide, 3C-6H transition, stacking faults, diffuse X-ray scattering

PACS: 61.72.Dd; 61.72Nn; 81.05.Hd

INTRODUCTION

Silicon carbide is a material exhibiting pronounced polytypism with more than 200 different structures. Among them, there is only one polytype with cubic symmetry (3C-SiC), which is a promising material for high-power and high-frequency electronic applications [1]. Nonetheless, the growth of 3C-SiC single crystals with a crystalline quality suitable for the applications aimed still remains an important issue. Indeed, growing SiC from the vapor phase requires temperatures higher than 1900°C [2], at which 3C-SiC is unstable [3]. This instability promotes the 3C-6H transitions through the multiplication and expansion of stacking faults (SFs) lying in the {111} planes. Since such SFs are detrimental to the electronic properties of 3C-SiC [1], a real development of 3C-SiC - based devices necessitates an optimisation of the crystals quality and hence a better understanding of the 3C-6H transition.

Because of the rarity of 3C-SiC single crystals, the 3C-6H transition in SiC has only been scarcely studied (see Ref. [3] and references therein) and the transformation kinetics are yet unknown. Up until recently even the transformation mechanism was not clearly identified. A previous study using diffuse X-ray scattering (DXS) revealed that the transformation implies the glide of partial dislocations [4], probably according to a mechanism first described by Pirouz (Ref. [5] and references therein). In the present work, we pursue these DXS experiments in order to analyse the 3C-6H polytypic transition on both a qualitative (i.e. what are the mechanisms involved) and quantitative (i.e. the transformation kinetics) standpoint.

The transformation does not affect the whole crystal but instead there are regions where the transition takes place and other that remain unaffected. We show that the simulation of

experimental DXS curves allow to determine both the volume fraction corresponding to the partially transformed regions and the transformation level within these regions. The evolution of these parameters with time and temperature provides invaluable information regarding the transformation mechanisms and transformation kinetics. The article is organized as follows: first we provide informations regarding the 3C-SiC single crystals and DXS data acquisition. The simulation procedure is then recalled. Finally the results are discussed. In particular, it is shown that the transition implies the multiplication and extension of partial dislocations. The kinetics and activation energies of each of these mechanisms are determined.

EXPERIMENTAL DETAILS

3C-SiC Samples

The 3C-SiC samples used are 10*10 mm² and 250 µm-thick pieces, produced by HAST corporation by chemical vapour deposition on "undulant" (001) Si substrate [6]. These samples contain stacking faults (SFs) lying in the {111} planes. Previous studies revealed that the SF distribution in these samples is anisotropic [6, 7]: the (-111) and (1-11) planes exhibit a high SF density, whereas the (111) and (-1-11) planes exhibit a low SF density. This feature is a direct consequence of the growth technique on an undulant Si substrate [6]. In the following we shall only consider the planes exhibiting a high SF density, since the 3C-6H transition mainly takes place in the direction normal to these planes. The samples considered in the following have been annealed at high temperatures in order to promote the 3C-6H transition. Two sets of samples have been analysed. In the first one, 3C-SiC single crystals have been annealed at 2000°C for a time ranging between 1h and 8h. In the second one, the crystals have been annealed during 5 hours at temperatures ranging between 1700°C and 2100°C. The annealing experiments were conducted under 60 kPa of Argon. The surface of the crystals is

slightly graphitized upon annealing. The graphite layer is removed before subsequent characterizations.

Reciprocal space mapping

Wide-range reciprocal space maps (RSMs) including the (002) and (-113) reflections of 3C-SiC have been recorded on a home-made laboratory diffractometer. It is based on a rotating Cu anode coupled with a four reflections Ge(220) monochromator and equipped with a curved position sensitive detector (PSD) with a 120° angular aperture. A five-movement sample holder allows precise sample positioning. The X-ray beam impinging on the sample is monochromatic (Cu $K\alpha_1$, $\Delta\lambda/\lambda=1.4\times10^{-4}$) and parallel in the detector plane ($\Delta\theta$=12 arcsec) with dimensions 10 × 0.1 mm^2 so that a large volume of the sample is analysed which provides statistically significant averaged values. A detailed description of the set-up has been given elsewhere [8]. A RSM represents the scattered intensity in a particular (Q_x, Q_z) plane, where Q_x and Q_z are the components of the scattering vector **Q** ($Q = 4\pi \sin\theta / \lambda$) in the crystal plane and perpendicular to it, respectively. In the following experiments, Q_x and Q_z have been set parallel to the [1-10] and the [001] directions of SiC.

The relationships between SiC polytypes are most easily understood when considering a common hexagonal unit-cell. In the following we shall hence make use of usual three-layer hexagonal unit cell (i.e. “3H” instead of 3C) where the $[001]_h$ direction (the subscript 'h' stand for 'hexagonal') is parallel to [111] direction of the cubic lattice. Notice that a given HKL_h reflection corresponds to the $HK\ 2L$ reflection in the actual 6H unit-cell. Figure 1a shows the correspondence between the reciprocal lattices of the cubic (black) and hexagonal (red) phases. It is noteworthy that the additional reflections corresponding to the 6H phase are localized along specific $[H0L]_h$ rows, with $H = 3n \pm 1$, where n is an integer (the row joining the cubic (002) and (-113) reflections being $[10L]_h$). During the polytypic transition the diffuse scattering will be concentrated along these rows, so that they can be used to monitor

the transition [9].

Two typical reciprocal space maps (corresponding to the shaded area in figure 1a) are displayed in figure 1b and 1c. Figure 1b corresponds to a raw (non-annealed) crystal: the (002) and (-113) Bragg peaks of the cubic phase are clearly visible and the diffuse scattering (due to randomly distributed SFs) is very weak. On the contrary, in figure 1c, corresponding to a significantly transformed crystal, the diffuse scattering is very pronounced and almost continuously connects the Bragg reflections (notice the two equivalent diffuse streaks corresponding to SFs lying in the (-111) and (1-11) planes). These reciprocal space maps have been recorded in ~ 8 hours (which corresponds to 0.01° incidence angle scanning step and 10 seconds counting time per step). In the following, the intensity distribution along the $[10L]_h$ row is extracted from the map so as to be simulated with the diffuse scattering model described below.

SIMULATION PROCEDURE

The 3C-6H transition implies a re-stacking from ABCABC to ABCACB and hence necessarily implies spatial correlations in the SF positions: three SFs occurring on three successive lattice planes are necessary to transform two 3C unit-cells into one 6H unit-cell. These spatial correlations between SFs result in the extended diffuse scattering observed along the $[10L]_h$ direction; its analysis hence provides informations about the transformation mechanism and the transformation level. Recently we developed a scattering model which allows to effectively fit experimental DXS curves. This model is very briefly recalled here (for more details, see [10,11]). The intensity distribution along the $[10L]_h$ row is written as follows :

$$I(L)=k(L)\int dL'\cdot R(L')I_s(L-L')+b$$

where the scale factor *k(L)* is a function including the irradiated volume, the polarisation factor and the intensity of the incident beam and *b* is the background. $I_s(L)$ is the intensity scattered from the sample which is convoluted with the resolution of the diffractometer $R(L)$ (for details see [8]). Optical birefringence microscopy observations (not shown here) revealed that the transformation does not affect the whole crystal: there are regions where the transformation significantly develops and other that remain in the 3C phase. The former give rise to diffuse scattering, $I_d(L)$, whereas the latter give rise to coherent scattering, $I_c(L)$, so that the intensity scattered from the sample is simply :

$$I_s(L) = x_t\, I_d(L) + (1\text{-}x_t)\, I_c(L)$$

where x_t is the volume fraction of transformed material. The coherent scattering $I_c(L)$ can be straightforwardly calculated assuming a particular mosaic domain shape and size [12]. The diffuse scattering $I_d(L)$ is calculated as detailed in [10] and is solely dependent on the transformation level τ within the transformed regions ($\tau = 0$ corresponds to 3C whereas $\tau = 1$ corresponds to 6H). This parameter is hence easily obtained by fitting the diffuse part of the scattered intensity. The volume fraction of transformed material x_t is obtained by matching the diffuse/coherent intensity ratio. The influence of these two parameters on the DXS curves is depicted in figure 2. The intense peaks located at $L = 2$ and $L = 5$ correspond to the coherent Bragg peaks emanating from the untransformed regions. The diffuse signal between the Bragg peaks originates from the partially transformed regions. Increasing the volume fraction of transformed material x_t (at a fixed transformation level τ) simply results in an increase of the diffuse intensity, figure 2a. On the contrary, increasing the transformation level τ (at a fixed volume fraction x_t) results in a structuring of the diffuse scattering in the form of pseudo-peaks, whereas the total diffuse intensity is approximately the same, figure 2b. Since these parameters have a very distinct influence on the DXS curves so that they can be easily

determined by fitting the data with the model described above. Example fits corresponding to crystals annealed 5 hours for increasing temperature are shown in figure 3. It can be seen that the model provides a fairly good description of the experimental data.

RESULTS AND DISCUSSION

The volume fraction x_t and the transformation level τ deduced from the simulations for all investigated crystals are displayed in figure 4. Figure 4a represents the evolution with time of τ and x_t at a temperature of 2000°C. Figure 4b represents the evolution of τ and x_t as a function of temperature in the form of an Arrhénius plot. Let us first consider the evolution with annealing time. The first striking observation is that the transformation level and the volume fraction are characterized by two very distinct kinetics. Whereas the transformation level exhibits a fast kinetic and reaches a value of 80 % after 8 hours, the volume fraction exhibits a much slower kinetic and only reaches 33 % after 8 hours. This observation suggests that these two evolutions imply two distinct mechanisms. The increase of the transformation level necessarily implies the creation of new SFs. It has been shown that new SFs can be created in SiC by the multiplication of partial dislocations using the double cross-slip mechanism [5]: successive lattice planes are faulted by an initial dissociated dislocation that slips from one lattice plane to the other. On the contrary, the increase of the volume fraction does not necessarily imply the creation of new SFs: the glide of partial dislocations in their planes produces an extension of the SFs that increases the volume fraction of transformed material. However, in order to fault significant regions of the crystal, these dislocations have to glide over several tens of micrometers, a path along which they might be pinned by structural defects. Moreover, two dislocations, gliding in two different glide planes (say (-111) and (1-11)) can not cross each other (since they correspond to two different orientations of the

upcoming 6H phase) so that the motion of one of the dislocation is stopped. These arguments might explain why the corresponding kinetic is much slower and does not reach very high values (contrarily to τ).

At this point it is worth noticing that since the transformation level τ is determined from the shape of the DXS, it is sensitive to the coherence of the beam and the coherence of the material. Monte-Carlo simulations (not shown here) revealed that, as soon as the transformation level reaches a few percents, the correlation length perpendicular to the {111} lattice planes is reduced to a few tens of nanometers, i.e. the value of τ is determined from regions of a few tens of nanometers-thick scattering independently of each other. The value of τ is therefore not (or only weakly) sensitive to the presence of structural defects that might inhibit the double cross-slip motion. On the contrary, the volume fraction is determined from the integrated intensity of the DXS. Hence, any defect inhibiting the glide of the dislocations will have a direct impact on the measured value of x_t.

More can be learned from the activation energies corresponding to each mechanism (figure 4b). The increase of τ is characterized by an activation energy E_a = 1.5 eV. Since the increase of τ necessarily implies the creation of new SFs, this activation energy simply correspond to the energy required to activate the double cross-slip motion. The increase of x_t is characterized by an activation energy approximately three time smaller (E_a = 0.54 eV). This demonstrates that it indeed implies a distinct mechanism than τ, and in particular a mechanism that requires a much smaller activation energy. Although the activation energies for the glide of partial dislocations in 3C-SiC are unknown, it is fair to think that the corresponding energy is smaller than for the double cross-slip motion which implies a significant core reconfiguration [5].

CONCLUSIONS

The 3C-6H polytypic transition in SiC has been studied by diffuse X-ray scattering.

Reciprocal space maps including a wide portion of the $[10L]_h$ row have been recorded on a high-resolution laboratory diffractometer. The intensity distribution along this row has been extracted from the reciprocal space maps and simulated with a scattering model including the contributions of partially transformed regions and untransformed regions, as well as the transformation level within the partially transformed regions. It has been shown that the 3C-6H polytypic transition in SiC actually involves two different mechanisms: the first one corresponds to the nucleation of new stacking faults through a double cross-slip motion of dissociated dislocations lying in the basal plane, and the second one corresponds to the expansion of partial dislocations. The former is a fast process and characterized by an activation energy of E_a = 1.5 eV, whereas the latter is a slow process and characterized by an activation energy of E_a = 0.54 eV.

REFERENCES

1. H. Nagasawa, M. Abe, K. Yagi, T. Kawahara, N. Hatta, Phys. Stat. Sol. (b) 245, No.7, 1272-1280, (2008).
2. D. Chaussende, F. Mercier, A. Boulle, F. Conchon, M. Soueidan, G. Ferro, A. Mantzari, A. Andreadou, E. K. Polychroniadis, C. Balloud, S. Juillaguet, J. Camassel, M. Pons., J. Cryst. Growth 310, 976-981, (2008).
3. N. W. Jepps, T. F. Page, Proc. Cryst. Growth Charact. 7, 259-307 (1983).
4. A. Boulle, J. Aube, I. Galben-Sandulache, D. Chaussende, Appl. Phys. Lett. *94*, 201904, (2009).
5. P. Pirouz, Sol. State Phenomena. 56, 107-132, (1997).
6. H. Nagasawa, K. Yagi, T. Kawahara, N. Hatta, Chem. Vap. Deposition 12, 502-508, (2006).
7. A. Boulle, D. Chaussende, F. Conchon, G. Ferro, O. Masson, J. Cryst. Growth 310, 982-987, (2008).
8. A. Boulle, O. Masson, R. Guinebretière, A. Lecomte, A. Dauger, J. Appl. Crystallogr. 35, 606-614, (2002).
9. B. I. Nikolin and A. Yu. Babkevich., Acta Cryst. A, 45, 797 -801, (1989).
10. A. Boulle, D. Dompoint, I. Galben-Sandulache, D. Chaussende, J.Appl. Cryst., 43, 867-875, (2010).
11. V. K. Kabra, D. Pandey, S. Lele, J. Mater. Sci., 21, 1654, (1986).
12. A. Boulle, F. Conchon, R. Guinebretière, Acta Crystallogr. A 62, 11-20, (2006).

List of figure captions

Figure 1: (a) Schematic representation of the cubic (black) and hexagonal (red) reciprocal lattices. The 3C-SiC reflections are represented as large gray spheres. The additional reflections of 6H-SiC are represented as small red spheres. The rectangle indicates the area scanned by reciprocal space mapping. (b) Typical reciprocal-space map of an untransformed crystals exhibiting the (002) and (-113) Bragg peaks and a very weak diffuse scattering. (c) Typical reciprocal-space map of a partially transformed 3C-SiC single-crystal. The diffuse streak joining the (002) and (-113) reflections is clearly visible. The angle $\psi = 54.74°$ is the angle between the {001} and the {111} planes of a cubic lattice.

Figure 2: Influence of the polytype volume fraction x_t (a) and the transformation level τ (b) on the DXS profiles. For these calculations τ (respectively x_t) is kept constant and equal to 20% while x_t (respectively τ) successively takes the following values: 0, 10, 40 and 70 %. The curves are normalized to the same maximum value. Increasing x_t results in a simple increase of the diffuse intensity, whereas increasing τ results in a structuring of the diffuse intensity.

Figure 3: Experimental (black continuous line) and simulated (red dotted line) intensity distribution along the $[10L]_h$ row. The samples have been annealed 5 hours at 1700, 1800, 1900 and 2100°C. The curves are shifted vertically for clarity.

Figure 4: (a) evolution of the transformation level τ and of the volume fraction x_t as a function of annealing time at 2000°C. The dotted line is a fit with a power-law. (b) Arrhénius plot of

the transformation level τ and volume fraction x_t. The annealing temperatures are 1700, 1800, 1900 and 2100°C and the annealing time is 5 hours.

Figures

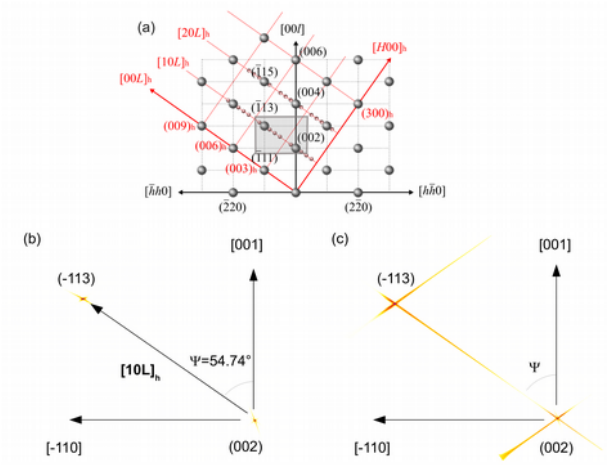

Figure 1

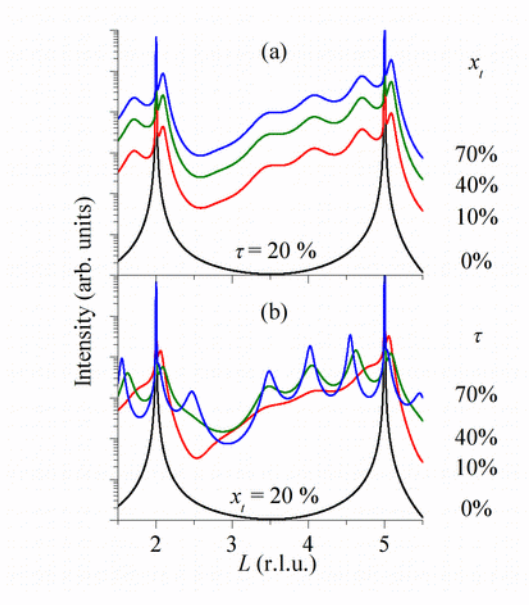

Figure 2

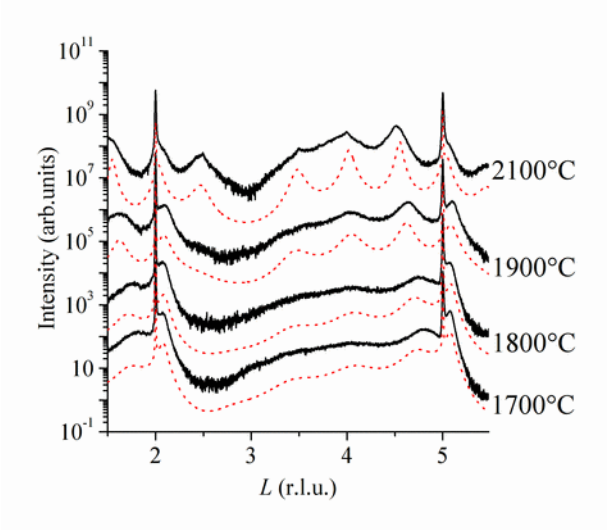

Figure 3

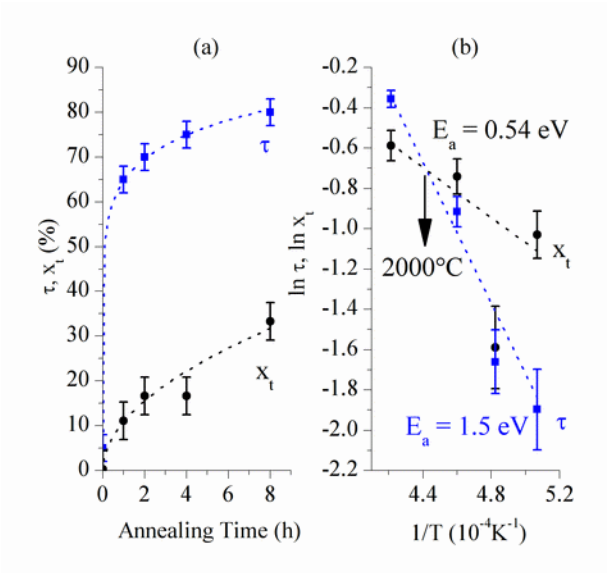

Figure 4